Chemical Bond Imaging using Higher Eigenmodes of Tuning Fork Sensors in Atomic Force Microscopy

Daniel Ebeling,[1, a)] Qigang Zhong,[1, 2] Sebastian Ahles,[3] Lifeng Chi,[2] Hermann A. Wegner,[3] and André Schirmeisen[1]

[1)] *Institute of Applied Physics (IAP), Justus Liebig University Giessen, Heinrich-Buff-Ring 16, 35392 Giessen, Germany*

[2)] *Institute of Functional Nano & Soft Materials (FUNSOM), Soochow University, 215123 Suzhou, P. R. China*

[3)] *Institute of Organic Chemistry, Justus Liebig University Giessen, Heinrich-Buff-Ring 17, 35392 Giessen, Germany*

(Dated: 19 April 2017)

We demonstrate the ability of resolving the chemical structure of single organic molecules using non-contact atomic force microscopy with higher normal eigenmodes of quartz tuning fork sensors. In order to achieve submolecular resolution CO-functionalized tips at low temperatures are used. The tuning fork sensors are operated in ultrahigh vacuum in the frequency modulation mode by exciting either their first or second eigenmode. Despite the high effective spring constant of the second eigenmode (on the order of several ten kN/m) the force sensitivity is sufficiently high to achieve atomic resolution above the organic molecules. This is observed for two different tuning fork sensors with different tip geometries (small tip vs. large tip). These results represent an important step towards resolving the chemical structure of single molecules with multifrequency atomic force microscopy techniques where two or more eigenmodes are driven simultaneously.

Recently, the so-called "bond imaging" atomic force microscopy (AFM) technique was introduced by Gross et al.[1], which allows to resolve the chemical structure of single adsorbed molecules on surfaces. This technique is based on functionalizing the AFM tip with a single CO molecule at low temperatures in order to boost the lateral resolution. This has attracted attention, in particular, in the field of on-surface chemistry, since it allows to study molecules and molecular structures at a new level of precision. Researchers have applied the method, e.g., to identify unknown molecular species, measure the length of inter- and intramolecular bonds, determine the bond order, and to investigate complete reaction pathways.[2–15]

Another recent development regarding dynamic AFM are the so-called "multifrequency" techniques, which are able to improve the imaging capabilities in different ways (see e.g. Ref.[16] for a review). In an early theoretical work Rodriguez et al.[17] proposed that the compositional image contrast can be enhanced by simultaneously exciting two normal eigenmodes of a standard silicon AFM cantilever. Shortly thereafter, the improvement of imaging capabilities was demonstrated experimentally on soft sample systems such as molecular islands or antibodies in air and liquids[18,19]. To date it has been shown that the multifrequency method is adaptable to different sample systems in various environments. Notably, for high resolution imaging in ultrahigh vacuum[20] and in liquids[21–23] it has been presented that driving the second eigenmode of silicon cantilevers at small amplitudes can significantly increase the signal-to-noise ratio. In general, these measurements require a careful choice of imaging parameters depending on the environment and sample system. In particular, the amplitude ratio of the first and second eigenmodes plays an important role for the image contrast. Amplitude ratios in the range of $A_2/A_1 = 1:1-1:200$ (see e.g.,[18,20,21,24,25]) have been reported to be beneficial for achieving optimal imaging conditions.

To resolve the chemical structure of single molecules via the bond imaging technique mainly low temperature AFMs equipped with quartz tuning fork sensors[26] are used (see Refs. above and Refs.[27,28] for rare exceptions). The normal stiffness of tuning fork sensors is, however, ≈ 50 times higher than typical values of standard silicon cantilevers (1800 vs. 40 N/m), which leads to an exceptionally high stiffness of the second eigenmode ($k_2 \approx (f_2^2/f_1^2)k_1 \approx 40k_1 \approx 72$ kN/m, where f_1, f_2 are the resonant frequencies of the first and second eigenmodes[16]).

Since the force gradient in the repulsive regime of the tip-sample interaction is usually on the order of a few N/m[30,31] the effective stiffness of the second eigenmode of a tuning fork sensor seems rather high for achieving force sensitivities that are needed for submolecular resolution imaging. However, Tung. et al.[32] studied the characteristics of higher-order eigenmodes of tuning fork sensors using theoretical modeling and scanning laser Doppler vibrometry. The authors suggest that driving higher eigenmodes of quartz tuning fork sensors is promising due to their unique properties (as discussed below). Moreover, it has been demonstrated that tuning fork sensors driven at higher eigenmodes are suitable to resolve the lattice structure of ionic crystal surfaces in vacuum[33] and in ambient conditions[34].

Here, we are presenting AFM measurements with CO-functionalized tips of single aromatic molecules at 5 K, which have been performed by exiting either the first

[a)] Daniel.Ebeling@ap.physik.uni-giessen.de

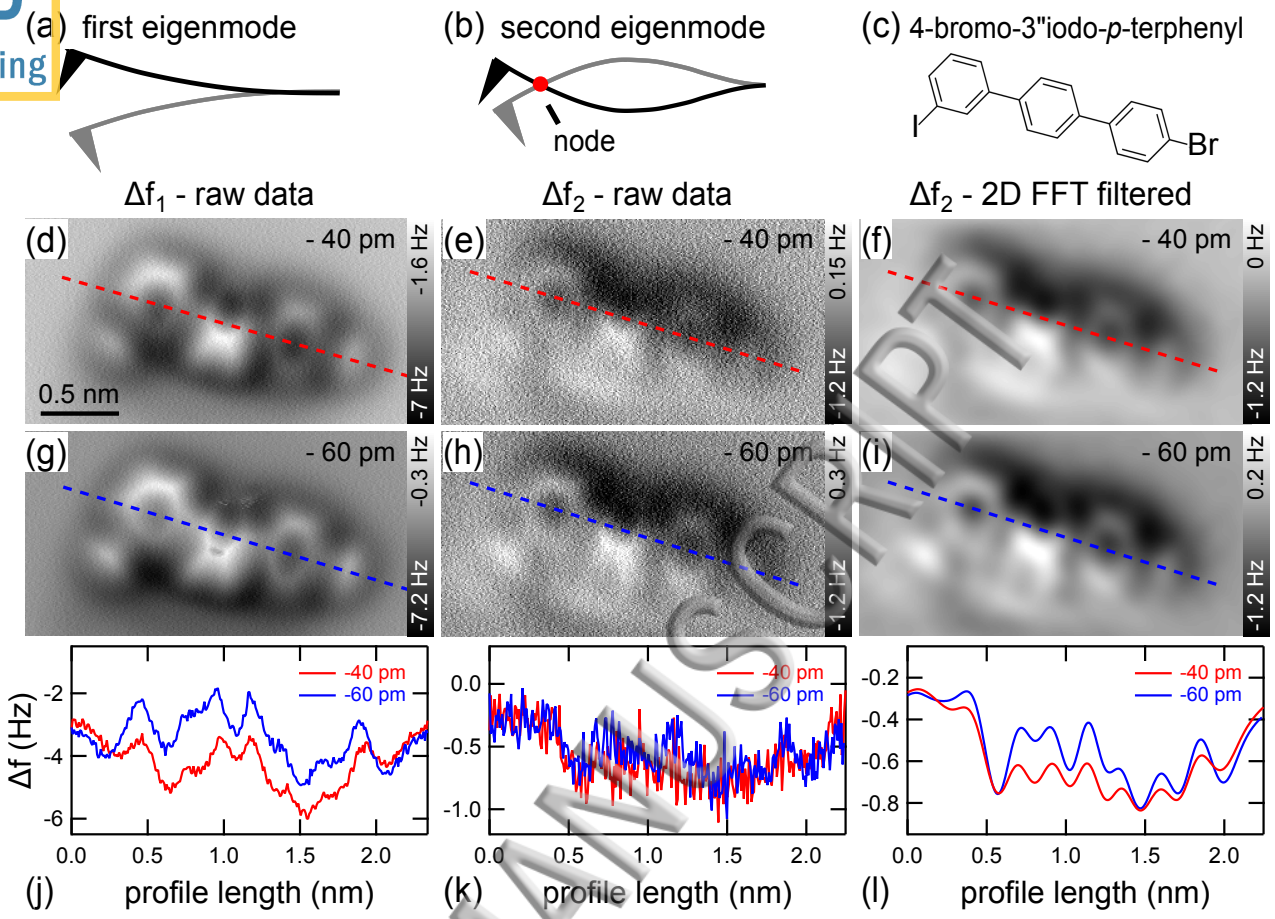

FIG. 1. (color online) Schematic drawing of the shapes of the first (a) and second (b) eigenmodes. The oscillation node of the second eigenmode is indicated by a red dot. (c) Chemical structure of 4-bromo-3-iodo-*p*-terphenyl. (d,g) AFM frequency shift images of first eigenmode at $\Delta z = -40$ pm and -60 pm showing a single 4-bromo-3-iodo-*p*-terphenyl molecule on Cu(111). (j) Corresponding line profiles at $\Delta z = -40$ pm (red line) and -60 pm (blue line). (e,h,k) Corresponding images and scanlines of second eigenmode. (f,i,l) Low pass 2D FFT filtered version of second eigenmode images (cutoff frequency ~ 6 nm^{-1}). Parameters: Quartz tuning fork sensor operated at 5 K in UHV conditions. $Amp_1 = 50$ pm, $f_1 = 27.0$ kHz, $Amp_2 = 50$ pm, $f_2 = 163.9$ kHz. The Δz-offsets are given with respect to the tunneling gap at $U_{\text{sample}} = 100$ mV and $I_{\text{set}} = 10$ pA (with oscillating tip). The oscillation amplitudes have been calibrated using the "constant current method" as described in Ref.[29]. PLL-bandwidth = 10 Hz, scanning velocity = 470 pm/s.

or the second normal eigenmode of two different quartz tuning fork sensors. We demonstrate, that the chemical structure of an adsorbed molecule can be clearly resolved by exciting higher eigenmodes. This paves the way for future studies on molecular systems using multifrequency techniques where two or more eigenmodes are driven simultaneously.

In general, multifrequency imaging offers a wider range of setting options, i.e., the imaging parameters of the different eigenmodes can be separately optimized for different purposes. In bimodal imaging, e.g., the two eigenmodes can be used for topographical imaging and compositional mapping, respectively[17]. This concept can even be extended to further eigenmodes, which are simultaneously driven.[35–37] As high-resolution scans with CO-tips are mainly performed in the constant height mode, this feature of the multifrequency method is in particular interesting for studies of molecular systems. The multifrequency technique opens up the possibility of achieving submolecular contrast while simultaneously tracking the sample topography.

All measurements have been performed at 5 K using a commercial low-temperature AFM (ScientaOmicron, Germany) and quartz tuning fork sensors. The aromatic molecules (4-bromo-3-iodo-*p*-terphenyl, cf. structure in Figure 1 (c) and Supplemental Material for detailed information about the synthesis) have been evaporated onto a clean and cold (< 100 K) Cu(111) substrate with a home-built evaporation setup (see Refs.[15,38] for further experimental details). Prior to CO-functionalization (as described by Bartels et al.[39]) the tungsten tip has been covered with substrate material and sharpened by several tip-sample indentations and voltage pulses.

Figure 1 (a,b) depicts schematic drawings of the shapes

of the first and second eigenmodes. For the used tuning fork sensor the following resonance frequencies and quality factors have been measured for the first and second eigenmodes: $f_1 = 27.0$ kHz, $f_2 = 163.9$ kHz and $Q_1 = 20700$, $Q_2 = 18400$. Figure 1 shows constant height frequency shift images of a single 4-bromo-3-iodo-*p*-terphenyl molecule on Cu(111), which have been obtained by either exciting the first (d,g) or the second eigenmode (e,h) for two different imaging heights ($\Delta z = -40$ and -60 pm with respect to tunneling gap at 100 mV gap voltage and 10 pA current setpoint). Corresponding line profiles for both eigenmodes at both imaging heights are presented in (j,k). In order to directly compare the imaging capabilities of the two eigenmodes the same imaging parameters and, in particular, the same oscillation amplitude of 50 pm and tip-sample distance has been used for the measurements.

The chemical structure of the 4-bromo-3-iodo-*p*-terphenyl molecule is revealed in both eigenmodes, i.e., both eigenmodes allow for identifying the position of the three phenyl rings and the precise location of the attached bromine and iodine atoms. As can be determined from the images and the corresponding scanlines the signal-to-noise ratio is significantly lower for the second eigenmode, which is due to its higher effective stiffness. The information about the chemical structure of the molecule, which is contained in the images, however, is comparable to the scans in the first eigenmode. This is illustrated by the 2D FFT filtered versions of the second eigenmode images (cf. Figure 1 (f,i,l)), which are in good agreement with the first eigenmode scans. Even the slight tilt of the middle phenyl ring with respect to the surface plane is revealed in both eigenmodes. Please note that the appearance of the dark halos around the molecules, however, is slightly different in the two eigenmodes. In the first eigenmode this dark halo is somewhat stronger at the bottom side of the molecule (cf. Figure 1 (g)), which is due to a slightly tilted CO-tip. For the second eigenmode the dark halo is more pronounced at the top side of the molecule.

As reported by Tung et al.[32] the added mass of the tip and even its geometry can have a significant influence on the force sensitivity of the second eigenmode, since it alters its shape. The authors observed that the oscillation node of the second eigenmode (see Fig. 1 b) is systematically moving outwards with increasing tip mass, which is accompanied by a reduction of oscillation amplitudes. Besides, it was found that the piezoelectric sensitivity of the tuning fork sensor is significantly affected by the tip geometry. The authors conclude that especially larger tips open up the possibility of obtaining unique properties but require a careful optimization of tip geometries. Hence, we performed additional experiments with a different tuning fork sensor with a different tip geometry. In this case the resonance frequency of the first eigenmode was $f_1 = 19.3$ kHz, which indicates that the mass of the attached tip was significantly larger than for the other sensor (27.0 kHz). According to the nomenclature introduced in Ref.[32] the two tip geometries used here are within the range of "regular" (29.7 kHz) and "large" (14.0 kHz) tips. Hence, in particular for the sensor with the larger tip an influence of the described effects is expected.

In Figure 2 we are presenting constant height frequency shift images, which are measured with the second tuning fork sensor (large tip, 19.3 kHz). The images are obtained by either exciting the first or the second eigenmode. In this case, our goal was to achieve the best imaging performance for each eigenmode independently. Hence, each eigenmode was driven with its smallest stable oscillation amplitude at an imaging height where good submolecular contrast is achieved. For the first eigenmode image an oscillation amplitude of 140 pm and a Δz-offset of -20 pm with respect to the tunneling setpoint (200 mV, 10 pA) was used. The second eigenmode images were taken with $Amp_2 = 10$ pm at two different Δz-offsets (-120 and -95 pm). Please note, as the excitation was switched on before stopping the STM feedback the Δz-offsets are not directly comparable in this case due to the different amplitudes of the different eigenmodes. The selected imaging region contains two 4-bromo-3-iodo-*p*-terphenyl molecules, which have been covalently coupled via the on-surface Ullmann reaction (see e.g., Ref.[15,40]). To trigger the Ullmann coupling between the two molecules the substrate was heated to 700 K for 10 min and subsequently cooled down to 5 K for imaging. Bromine and iodine atoms are homolytically cleaved from the terphenyl molecules during the Ullmann reaction and represent the majority of adsorbed atomic species on the surface.

Also with this sensor it is possible to image the chemical structure of the coupled terphenyl molecules (cf. Figure 2 (f)) with both operation modes, i.e., either by exciting the first or the second eigenmode. A direct comparison of the second eigenmode performance of the two different tuning fork sensors (cf. Figure 1 (e,h) and Figure 2 (b,c)) reveals an increased image quality for the sensor with the larger tip. In particular, for the second eigenmode image at $\Delta z = -120$ pm (Figure 2 (b)) a remarkable image contrast is achieved. In this case certain features in the images such as the transitions between bright and dark regions or single bromine and iodine atoms next to the molecules (indicated by red an blue arrows) appear even somewhat sharper than in the first eigenmode image. In particular, the two atoms marked by blue arrows are clearly discernible in Figure 2 (b), which is barely the case for Figure 2 (a) or (c).

The line profiles in Figure 2 (d,e) reveal that the absolute frequency shift noise is higher for the second eigenmode. However, also the magnitude of the frequency shift contrast, which is observed above the molecules is higher for the second eigenmode operation (cf. black dashed and solid lines in (d,e), which indicate the average frequency shift and the observed range of the frequency shift values above the molecules). Overall, the imaging performance for the tuning fork sensor with the larger tip is promising for the used imaging conditions. For a final classifica-

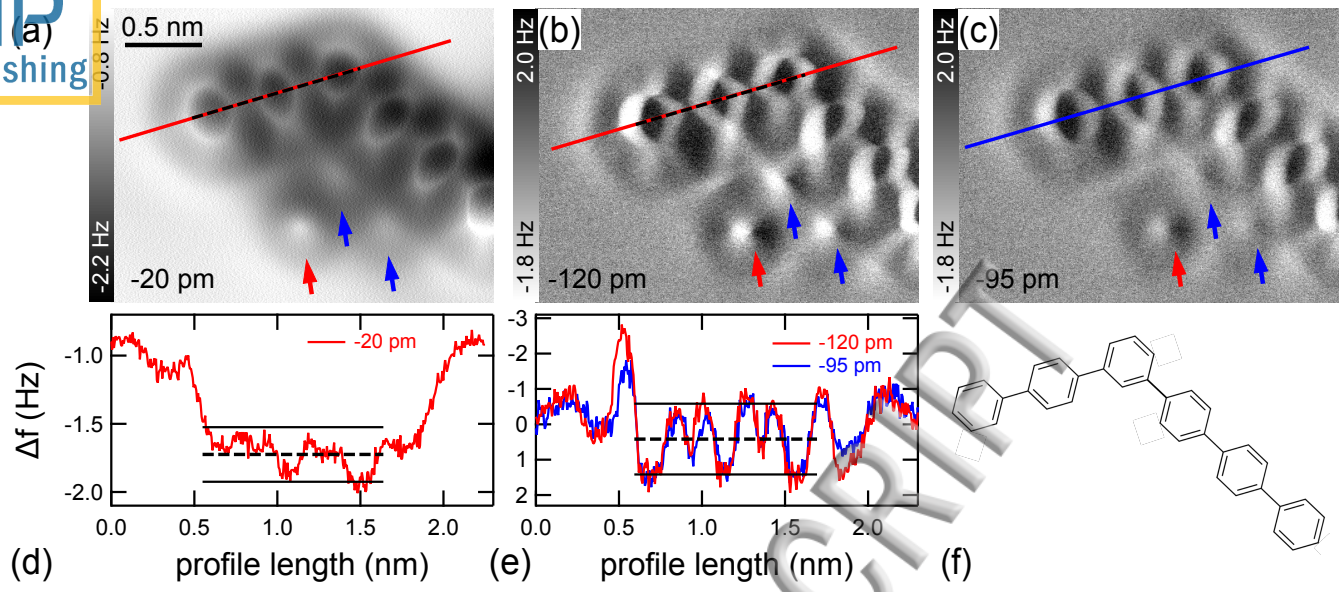

FIG. 2. (color online) Constant height frequency shift images of terphenyl molecules obtained by either exiting the first (a) or the second (b,c) eigenmode. Please note that (b,c) are displayed with inverted color scheme (see text for details). Bromine and iodine atoms are marked by red and blue arrows. (d,e) Line profiles extracted from images (a-c). The red and blue solid lines in the corresponding images indicate the profile path. The dashed and solid black lines indicate the average frequency shift above the molecule and its upper and lower bounds, respectively. (f) Molecular structure of two coupled terphenyl molecules. Parameters: $Amp_1 = 140$ pm, $f_1 = 19.3$ kHz, $\Delta z_1 = -20$ pm, $Amp_2 = 10$ pm, $f_2 = 177.9$ kHz, $\Delta z_2 = -120$ pm (b) and -95 pm (c). The Δz-offsets are given with respect to the tunneling gap at $U_{\text{sample}} = 200$ mV and $I_{\text{set}} = 10$ pA (with oscillating tip). PLL-bandwidth = 10 Hz, scanning velocity = 330 pm/s.

tion of the performance, however, a more comprehensive study with a systematical variation of imaging parameters is needed (see e.g., Ref.[21]).

This tuning fork sensor (large tip) offers the possibility to use extremely small oscillation amplitudes in the second eigenmode ($\sim$ 10 pm). Presumably this is related to the mentioned movement of the oscillation node for large tip geometries and responsible for the remarkable image contrast in the second eigenmode. Increased experimental sensitivity for decreasing oscillation amplitudes has been reported before (see e.g., Refs.[21,22,31,41]). Apparently, the sensitivity of an harmonic oscillator is, in first approximation, determined by the product of spring constant and amplitude kA. This can be followed from inspecting the dimensionless equation of motion of a damped harmonic oscillator (as discussed in Ref.[35]). Thus, the small amplitude, which can be used in the second eigenmode of this respective tuning fork sensor is compensating for its high effective stiffness.

Please note, while the tuning fork sensor with the larger tip offers a remarkable imaging performance in the higher eigenmode we also observe contrast inversion in the frequency shift signal. In order to directly compare the imaging capabilities of the first and second eigenmodes the images in Figures 2 (b,c) are displayed with an inverted color scheme (please see Supplementary Material for non-inverted image). When imaging single molecules using the bond imaging method the intramolecular bonds usually appear as bright lines (cf. Figure 2 (a)), which is attributed to short range repulsive tip-sample forces (i.e., induced by Pauli repulsion or short range electrostatics[1,42–45]), which lead to positive frequency shifts. In the second eigenmode image, however, we observe more positive frequency shift values above the center of the phenyl rings than above their rim (cf. Figures 2 (b,c) and Figure S1 in supplementary material).

At this point the underlying process of the contrast inversion in the second eigenmode remains unclear. Presumably, the observed effect is related to a number of different experimental parameters such as the extremely small oscillation amplitude, the accompanying small average tip-sample distance, the tip geometry which influences the mode shape, and the flexibility of the CO tip (see e.g., Refs.[4,46,47]). Hence, systematic studies with different experimental parameters are needed in order to reveal under which circumstances this contrast inversion occurs and if it is of general nature or if it is just a feature of the specific tuning fork sensor used. Next to identifying the underlying process of the contrast inversion such a study is also needed to reliably determine the optimum imaging conditions of the second eigenmode.

In conclusion, we were able to image the chemical structure of single molecules by driving a higher eigenmode of two different tuning fork sensors with different tip geometries (small tip vs. large tip). In particular,

for the larger tip and optimized imaging parameters a remarkable image contrast was achieved. Gaining deeper understanding about the underlying mechanisms (optimum imaging conditions, influence of tip geometry, contrast inversion, ect.) will be very useful for designing further experiments.

The results presented here are interesting for future AFM studies with submolecular resolution using multifrequency techniques, where two or more eigenmodes are driven simultaneously. The technical implementation of this method is rather simple since no changes in the basic experimental setup are needed. An additional drive electronics is sufficient to run those experiments. Since, bond imaging experiments are usually performed in the constant height mode the multifrequency technique will offer the experimentalist additional control parameters, which could, e.g., be used to track the sample topography while simultaneously achieving submolecular contrast. This would be an important advancement for the exciting field of chemical structure analysis on surfaces, in particular, for imaging small 3D objects such as bulky molecules.

See Supplementary Material for non-inverted second eigenmode image and detailed information about the synthesis of 4-Bromo-3"iodo-*p*-terphenyl.

This project was supported by the Laboratory of Materials Research (LaMa) of JLU. We acknowledge financial support within the LOEWE program of excellence of the Federal State of Hessen (project initiative STORE-E). Financial support is provided by the DFG via the GRK (Research Training Group) 2204 "Substitute Materials for sustainable Energy Technologies". Q.Z. acknowledges financial support from the Soochow University Graduate Student International Exchange Scholarship.

[1] L. Gross, F. Mohn, N. Moll, P. Liljeroth, and G. Meyer, Science **325**, 1110 (2009).
[2] L. Gross, Nat. Chem. **3**, 273 (2011).
[3] M. P. Boneschanscher, J. van der Lit, Z. Sun, I. Swart, P. Liljeroth, and D. Vanmaekelbergh, ACS Nano **6**, 10216 (2012).
[4] L. Gross, F. Mohn, N. Moll, B. Schuler, A. Criado, E. Guitián, D. Peña, A. Gourdon, and G. Meyer, Science **337**, 1326 (2012).
[5] F. Albrecht, M. Neu, C. Quest, I. Swart, and J. Repp, J. Am. Chem. Soc. **135**, 9200 (2013).
[6] J. Zhang, P. Chen, B. Yuan, W. Ji, Z. Cheng, and X. Qiu, Science **342**, 611 (2013).
[7] D. G. de Oteyza, P. Gorman, Y.-C. Chen, S. Wickenburg, A. Riss, D. J. Mowbray, G. Etkin, Z. Pedramrazi, H.-Z. Tsai, A. Rubio, M. F. Crommie, and F. R. Fischer, Science **340**, 1434 (2013).
[8] A. Sweetman, S. P. Jarvis, P. Rahe, N. R. Champness, L. Kantorovich, and P. Moriarty, Phys. Rev. B **90**, 165425 (2014).
[9] T. Dienel, S. Kawai, H. Söde, X. Feng, K. Müllen, P. Ruffieux, R. Fasel, and O. Gröning, Nano Lett. **15**, 5185 (2015).
[10] M. Emmrich, F. Huber, F. Pielmeier, J. Welker, T. Hofmann, M. Schneiderbauer, D. Meuer, S. Polesya, S. Mankovsky, D. Ködderitzsch, H. Ebert, and F. J. Giessibl, Science **348**, 308 (2015).
[11] N. Pavliček, B. Schuler, S. Collazos, N. Moll, D. Pérez, E. Guitián, G. Meyer, D. Peña, and L. Gross, Nat. Chem. **7**, 623 (2015).
[12] J. Krüger, N. Pavliček, J. M. Alonso, D. Pérez, E. Guitián, T. Lehmann, G. Cuniberti, A. Gourdon, G. Meyer, L. Gross, F. Moresco, and D. Peña, ACS Nano **10**, 4538 (2016).
[13] A. Riss, A. P. Paz, S. Wickenburg, H.-Z. Tsai, D. G. De Oteyza, A. J. Bradley, M. M. Ugeda, P. Gorman, H. S. Jung, M. F. Crommie, A. Rubio, and F. R. Fischer, Nat. Chem. **8**, 678 (2016).
[14] Z. Majzik, A. B. Cuenca, N. Pavliček, N. Miralles, G. Meyer, L. Gross, and E. Fernández, ACS Nano **10**, 5340 (2016).
[15] S. Zint, D. Ebeling, T. Schlöder, S. Ahles, D. Mollenhauer, H. A. Wegner, and A. Schirmeisen, ACS Nano (2017), 10.1021/acsnano.7b01109.
[16] R. Garcia and E. T. Herruzo, Nat. Nanotechnol. **7**, 217 (2012).
[17] T. Rodriguez and R. Garcia, Appl. Phys. Lett. **84**, 449 (2004).
[18] N. F. Martinez, S. Patil, J. R. Lozano, and R. Garcia, Appl. Phys. Lett. **89**, 153115 (2006).
[19] N. F. Martinez, J. R. Lozano, E. T. Herruzo, F. Garcia, C. Richter, T. Sulzbach, and R. Garcia, Nanotechnology **19**, 384011 (2008).
[20] S. Kawai, T. Glatzel, S. Koch, B. Such, A. Baratoff, and E. Meyer, Phys. Rev. Lett. **103**, 220801 (2009).
[21] D. Ebeling and S. D. Solares, Nanotechnology **24**, 135702 (2013).
[22] D. Ebeling and S. D. Solares, Beilstein J. Nanotechnol. **4**, 198 (2013).
[23] T. Meier, B. Eslami, and S. D. Solares, Nanotechnology **27**, 085702 (2016).
[24] A. M. Gigler, C. Dietz, M. Baumann, N. F. Martinez, R. Garcia, and R. W. Stark, Beilstein J. Nanotechnol. **3**, 456 (2012).
[25] S. Patil, N. F. Martinez, J. R. Lozano, and R. Garcia, J. Mol. Recognit. **20**, 516 (2007).
[26] F. J. Giessibl, Applied Physics Letters **73**, 3956 (1998).
[27] C. Moreno, O. Stetsovych, T. K. Shimizu, and O. Custance, Nano Letters **15**, 2257 (2015).
[28] K. Iwata, S. Yamazaki, P. Mutombo, P. Hapala, M. Ondracek, P. Jelinek, and Y. Sugimoto, Nature Communications **6** (2015).
[29] G. H. Simon, M. Heyde, and H.-P. Rust, Nanotechnology **18**, 255503 (2007).
[30] G. Cross, A. Schirmeisen, A. Stalder, P. Grütter, M. Tschudy, and U. Dürig, Phys. Rev. Lett. **80**, 4685 (1998).
[31] H. Hölscher, A. Schwarz, W. Allers, U. D. Schwarz, and R. Wiesendanger, Phys. Rev. B **61**, 12678 (2000).
[32] R. C. Tung, T. Wutscher, D. Martinez-Martin, R. G. Reifenberger, F. Giessibl, and A. Raman, J. Appl. Phys. **107** (2010).
[33] A. Bettac, J. Koeble, K. Winkler, B. Uder, M. Maier, and A. Feltz, Nanotechnology **20**, 264009 (2009).
[34] H. Ooe, D. Kirpal, D. S. Wastl, A. J. Weymouth, T. Arai, and F. J. Giessibl, Applied Physics Letters **109**, 141603 (2016).
[35] D. Ebeling, B. Eslami, and S. D. J. Solares, ACS Nano **7**, 10387 (2013).
[36] S. D. Solares, S. An, and C. J. Long, Beilstein Journal of Nanotechnology **5**, 1637 (2014).
[37] S. An, S. D. Solares, S. Santos, and D. Ebeling, Nanotechnology **25**, 475701 (2014).
[38] S. Zint, D. Ebeling, S. Ahles, H. A. Wegner, and A. Schirmeisen, J. Phys. Chem. C **120**, 1615 (2016).
[39] L. Bartels, G. Meyer, and K.-H. Rieder, Appl. Phys. Lett. **71**, 213 (1997).
[40] L. Grill, M. Dyer, L. Lafferentz, M. Persson, M. V. Peters, and S. Hecht, Nat. Nanotechnol. **2**, 687 (2007).
[41] F. Giessibl, H. Bielefeldt, S. Hembacher, and J. Mannhart, Applied Surface Science **140**, 352 (1999).
[42] M. Schneiderbauer, M. Emmrich, A. J. Weymouth, and F. J. Giessibl, Phys. Rev. Lett. **112**, 166102 (2014).
[43] C.-S. Guo, X. Xin, M. A. V. Hove, X. Ren, and Y. Zhao, J. Phys. Chem. C **119**, 14195 (2015).
[44] M. Ellner, N. Pavliček, P. Pou, B. Schuler, N. Moll, G. Meyer, L. Gross, and R. Peréz, Nano Lett. **16**, 1974 (2016).
[45] J. van der Lit, F. Di Cicco, P. Hapala, P. Jelinek, and I. Swart, Phys. Rev. Lett. **116**, 096102 (2016).
[46] N. Pavliček, B. Fleury, M. Neu, J. Niedenführ, C. Herranz-Lancho, M. Ruben, and J. Repp, Phys. Rev. Lett. **108**, 086101 (2012).
[47] P. Hapala, G. Kichin, C. Wagner, F. S. Tautz, R. Temirov, and P. Jelínek, Phys. Rev. B **90**, 085421 (2014).

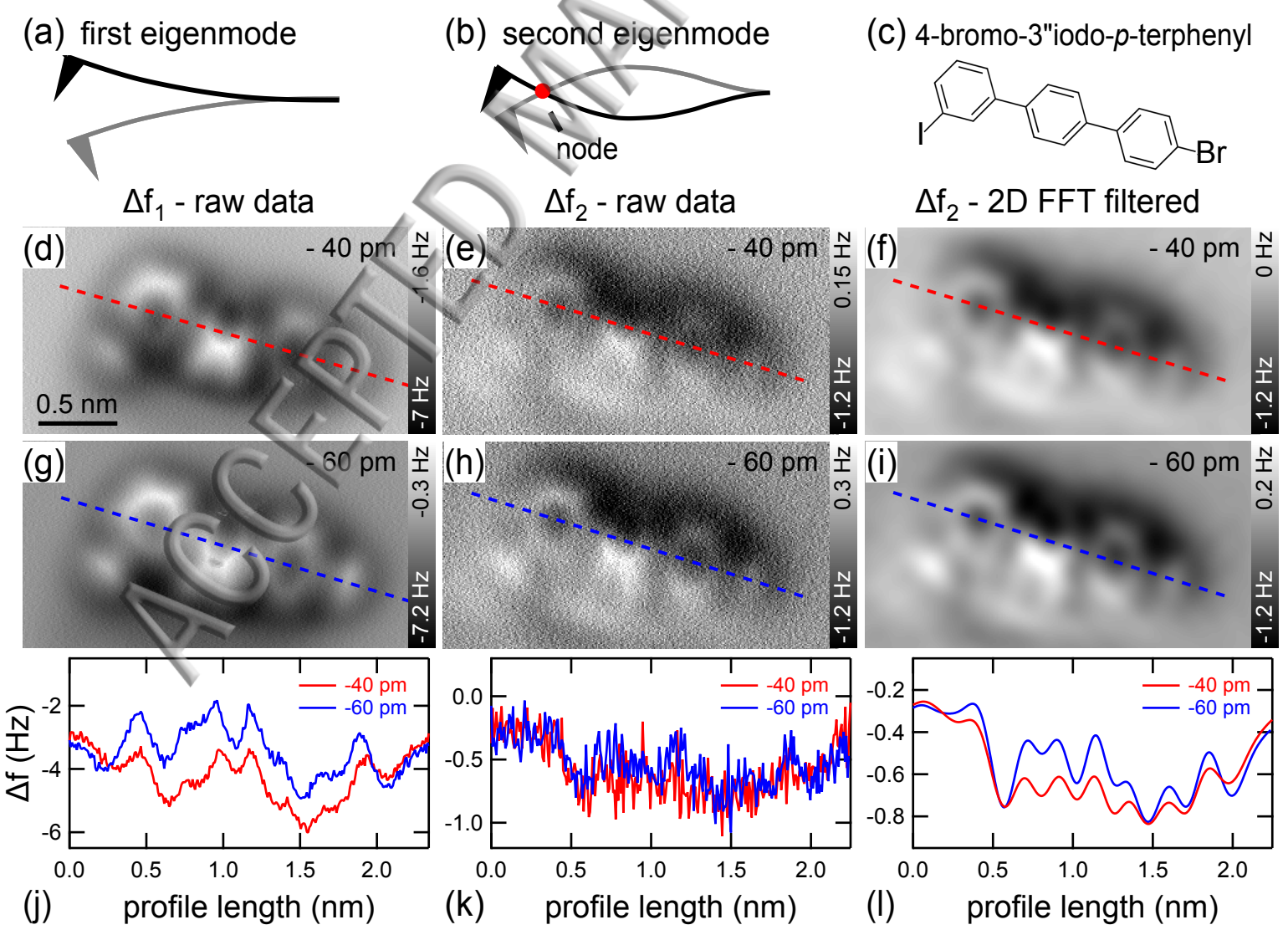

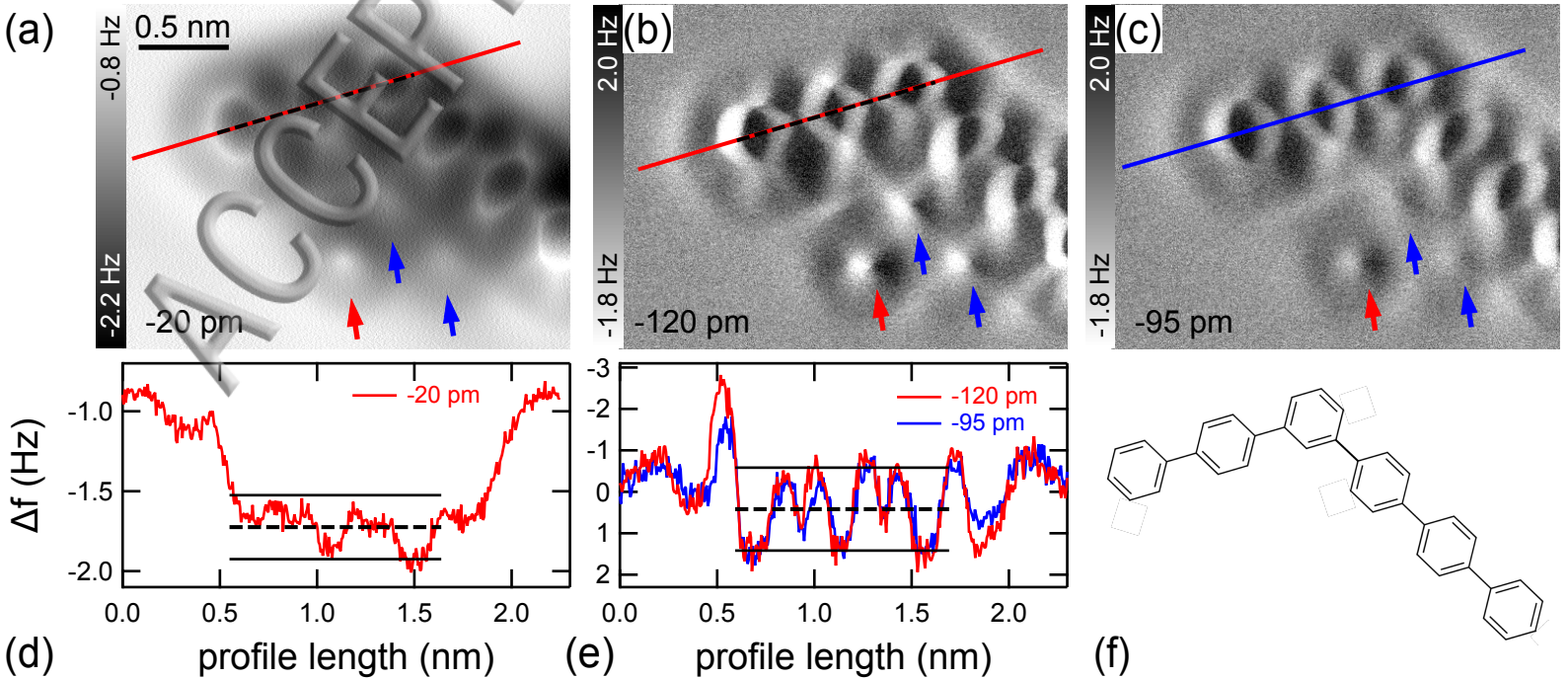
(a)
0.5 nm
-0.8 Hz
-2.2 Hz
-20 pm
(b)
2.0 Hz
-1.8 Hz
-120 pm
(c)
2.0 Hz
-1.8 Hz
-95 pm
Δf (Hz)
-20 pm
-120 pm
-95 pm
profile length (nm)
(d)
(e)
(f)